


## Article

# The Numerical Simulation and Experimental Investigation of the Laser Quenching Process of GCr15 Joint Bearings

Xiuli Yang<sup>1,2</sup>, Hao Zhang<sup>3</sup>, Dongliang Jin<sup>4,5</sup>, Xiqiang Ma<sup>3,4,\*</sup>  and Maolin Cheng<sup>2</sup><sup>1</sup> School of Engineering, Ocean University of China, Qingdao 266000, China; yangxiuli@ccccltd.cn<sup>2</sup> CCCC Second Harbor Engineering Co., Ltd., Wuhan 400430, China; chengmaolin@ccccltd.cn<sup>3</sup> School of Mechatronics Engineering, Henan University of Science and Technology, Luoyang 471003, China; 18461008951@163.com<sup>4</sup> Longmen Laboratory, Luoyang 471003, China; ziranheping@163.com<sup>5</sup> National Joint Engineering Research Center for Abrasion Control and Molding of Metal Materials, Luoyang 471003, China

\* Correspondence: maxiqiang@haust.edu.cn

**Abstract:** Joint bearings are widely used in modern industry in order to improve the mechanical properties of the outer surface of its inner ring. A laser quenching experiment was carried out in this paper. First of all, an experimental investigation was conducted on GCr15 ball-bearing material utilizing laser quenching, focusing on the effects of laser irradiation angles ranging from 0° to 10° and laser power levels between 600 W and 1100 W on the degree of hardening and microstructural alterations of the bearing material. Additionally, a reliable finite element analysis model was developed to assess the temperature field throughout the process. The findings indicate that an inclined laser enhances the stability of the hardened layer. Specifically, the hardening effect is minimal when the laser power is below 700 W, and optimal hardening is observed at power levels between 800 W and 900 W. During the laser quenching process when the temperature of the bearing material surpasses Ac1, the cooling rate can exceed 1700 °C/s. In regions where the peak temperature exceeds Ac1, the microstructure will undergo refinement, resulting in a reduction in the size of the martensite and a significant decrease in the number of carbides. In addition, the hardness value of these regions can be increased by 6 to 8 HRC, and the thickness of the quenching layer may exceed 0.3 mm. In the temperature range between Ac1 and Ms, the bearing material undergoes tempering, resulting in lower hardness compared to the base material, along with larger martensite and carbide particles. Furthermore, when using the overlap technique during the laser quenching, there will be a tempering zone both inside and on the surface of the bearing; meanwhile, the heat zones generated by different passes of the laser may have partly interacted, and the hardened zone generated by the previous pass may undergo tempering again.

**Keywords:** laser quenching; GCr15 joint bearing; finite element analysis; hardness; tempering



Academic Editor: Avik Samanta

Received: 6 January 2025

Revised: 25 January 2025

Accepted: 29 January 2025

Published: 1 February 2025

**Citation:** Yang, X.; Zhang, H.; Jin, D.; Ma, X.; Cheng, M. The Numerical Simulation and Experimental Investigation of the Laser Quenching Process of GCr15 Joint Bearings. *Coatings* **2025**, *15*, 158. <https://doi.org/10.3390/coatings15020158>

*Coatings* **2025**, *15*, 158. <https://doi.org/10.3390/coatings15020158>

**Copyright:** © 2025 by the authors. Licensee MDPI, Basel, Switzerland. This article is an open access article distributed under the terms and conditions of the Creative Commons Attribution (CC BY) license (<https://creativecommons.org/licenses/by/4.0/>).

## 1. Introduction

Spherical plain bearings are widely used in various industries and have been important basic components in chemical, shipbuilding, engineering machinery, mining, power generation, and other fields. Consequently, the effective extension of their operational lifespan holds significant research importance, and the surface characteristics of the inner ring serve as critical parameters influencing their friction and wear performance [1,2]. There have been many scholars who have explored this domain.

Laser quenching technology is a hot spot technology that utilizes a laser to enhance the surface properties of materials. This approach leverages the benefits of high energy density and localized modification of laser beams to attain superior quenching effects on metals, consequently enhancing the hardness, wear resistance, and corrosion resistance of the material [3,4]. It has attracted widespread attention in the field of bearing strengthening.

The surface hardening layer produced by laser quenching technology is finer and more uniform in structure than that produced by traditional quenching techniques [5,6]. Nonetheless, the optimal hardening parameters vary significantly across different materials and structures. Consequently, investigating the laser hardening parameters is a crucial step in the implementation of this technology [7]. In this process, comparing the hardening degree and microstructure of samples obtained under different strengthening parameters is the most common method [8,9]. Some researchers have also replaced the single-factor experiment with an orthogonal experiment to reduce the workload of the experiment and successfully predicted the optimal strengthening parameters [10,11]. In addition, by simulating the laser quenching process using finite element analysis software to obtain optimal strengthening parameters, the workload of experiments can be reduced. However, this procedure typically necessitates the development of a dependable thermal–mechanical coupling simulation model, as well as the assessment of the model’s reliability through empirical data [12,13].

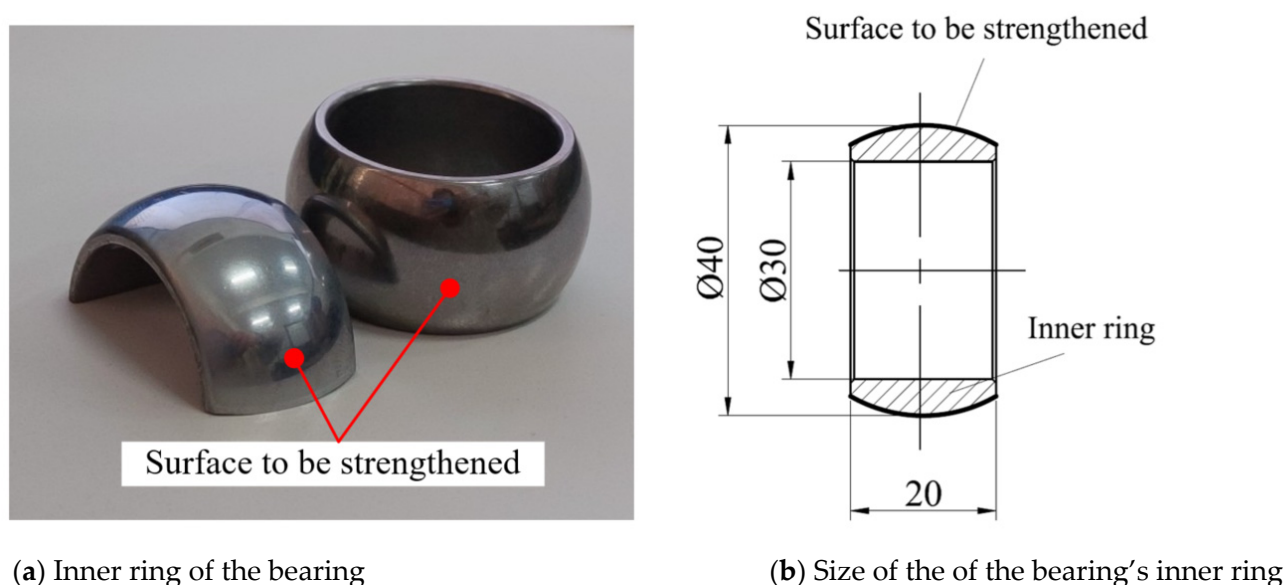
Some researchers focus on enhancing the wear resistance of materials through the process of laser quenching. To evaluate the effectiveness of the strengthened materials, they conducted experiments assessing friction and wear performance. The results show that laser quenching technology has a good improvement in the wear resistance of materials [14–17]. Some researchers also combine laser quenching technology with other surface treatment technologies to achieve a greater improvement in the surface properties of materials [18]. After laser quenching, there is a transition layer below the hardened surface layer. The hardness of this region is inferior to that of the substrate, prompting several researchers to investigate the mechanisms underlying the formation of this transition layer, as well as the potential methods for its enhancement [19–21].

Numerous investigations conducted by researchers have demonstrated that laser quenching can induce a strengthening effect on the surfaces of metals, but these studies are often for plates and bars, and research on spherical-bearing materials is relatively rare. It should be noted that the optimal parameters for achieving this strengthening effect differ across various materials and structures. Furthermore, at the microscopic level, the microstructural characteristics of the different subjects studied after strengthening exhibit distinct variations. Based on the above analysis, this study focuses on the inner ring of the GCr15 joint bearing as the primary subject of investigation. A laser quenching test is performed on this component, and a finite element analysis model of the quenching process is developed. By integrating the hardness distribution observed in the test sample with the temperature distribution derived from the simulation results, the mechanisms underlying laser quenching strengthening are examined, leading to the identification of optimal strengthening parameters. By analyzing the temperature field in the transition zone and comparing the microstructures of each region, the mechanism of the transition zone is studied. Finally, according to the research content of this paper, some characteristics and application suggestions of laser quenching technology are summarized.

## 2. Materials and Methodology

### 2.1. Materials

The inner ring of the knuckle bearing used in this study (which is manufactured by Fujian Longxi Bearing (Group) Co., Ltd., Zhangzhou, China) is shown in Figure 1a, and its dimensions are detailed in Figure 1b. This inner ring is composed of GCr15 steel, and the primary chemical composition of this material is outlined in Table 1. Prior to undergoing laser quenching treatment, the inner ring has already been subjected to quenching and finishing processes by the manufacturer. The outer surface of the inner ring is the area to be strengthened in this paper. Notably, the surface hardness of this region is marginally lower than that of the matrix material, measuring  $56 \pm 0.5$  HRC, with a depth of approximately 0.05 mm. In contrast, the hardness of the matrix material beneath the surface is about  $59 \pm 1$  HRC. Additionally, the surface roughness of the material ranges from 0.48 to 0.72  $\mu\text{m}$ . The outer surface of the bearing inner ring is spherical.



(a) Inner ring of the bearing

(b) Size of the of the bearing's inner ring

**Figure 1.** The inner ring of the GCr15 knuckle bearing used in this study.

**Table 1.** Main chemical composition of GCr15 bearing inner ring material used in the test.

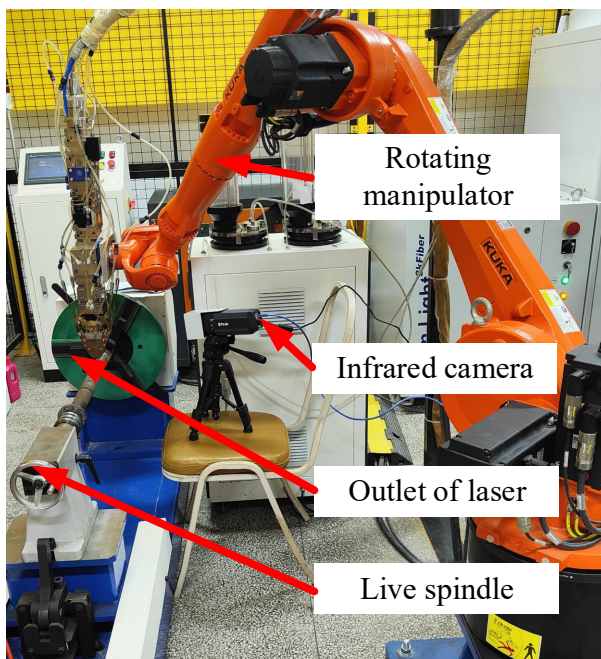
| Ingredient       | C         | Mn        | Si        | S                | P                 | Cr        |
|------------------|-----------|-----------|-----------|------------------|-------------------|-----------|
| Proportion (wt%) | 0.95~1.05 | 0.20~0.40 | 0.15~0.35 | $\leq \leq 0.02$ | $\leq \leq 0.027$ | 1.30~1.65 |

### 2.2. Research Programme

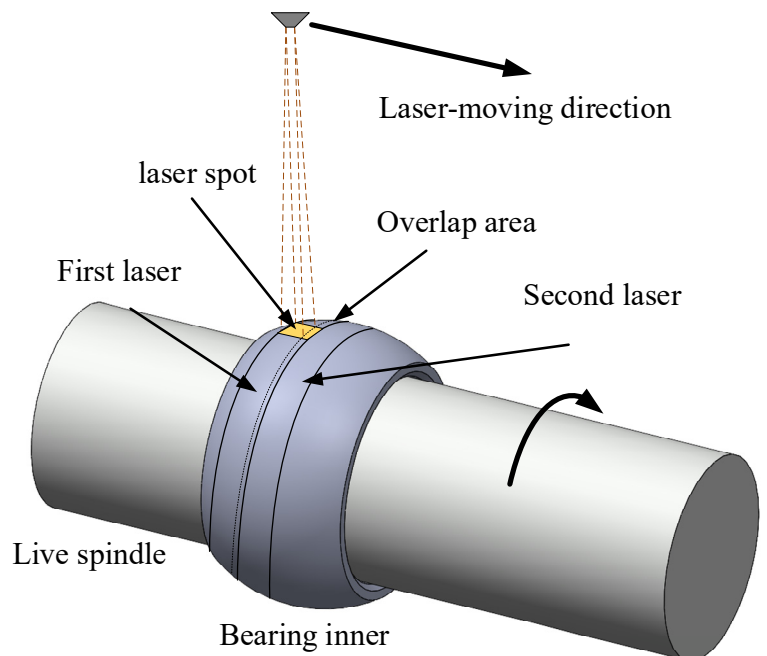
#### 2.2.1. Laser Quenching Experiment

This study utilizes industrial robots (KR 20 R1810-2, KUKA Robotics Corporation, Dalian, China) in conjunction with a laser additive manufacturing system, which includes an optical fiber laser (All-In-Light 3 kW, Precitrame Machines SA, Shenzhen, China) and supplementary components, to conduct laser hardening tests on the inner ring of a joint bearing. The main components of the system include the laser generation center, mechanical arm, and work axis system. During the experiment, the high-energy laser beam was emitted from the laser generation center and the laser power could be adjusted. The laser exit is located at the end of the mechanical arm, and the mechanical arm can realize the setting of the laser trajectory according to the input motion instructions. The workpiece is clamped on the work axis system to realize rotary motion and clamping. In order to obtain the surface temperature of the workpiece during laser quenching, an infrared temperature

camera (A615, FLIR Systems, Inc., Beijing, China) was used to detect the temperature of the workpiece in real time. The experimental site is shown in Figure 2a, and Figure 2b presents a schematic representation of the laser’s trajectory and the associated reinforcement procedure. In this study, the first circle of laser scanning is referred to as the ‘first laser’, and the second circle is referred to as the ‘second laser’. When the width or diameter of the laser spot is smaller than the surface area of the workpiece to be processed, the implementation of laser overlap is required. The overlap rate is defined as the ratio of the width of the overlap area to the width of the laser spot. In this study, the overlap rate is established at 20%. This paper investigates the strengthening principles of laser quenching on the subject of study, focusing on two key parameters: laser power and the angle of laser irradiation. In this study, the ambient temperature was Standard Temperature (20~30 °C) and pressure, and the air humidity was 25%~50%. Six distinct parameters for laser power have been established, specifically 600, 700, 800, 900, 1000, and 1100. Additionally, two angles of laser irradiation have been selected, namely 0° and 10°. The laser scanning speed is maintained at 15 mm/min, while the laser overlap rate is set at 20%. The parameters involved in the experiment are shown in Table 2.



(a) Equipment for laser quenching



(b) Schematic diagram of laser’s scanning mode

Figure 2. Principle of laser hardening.

Table 2. Parameter setting during the laser quenching experiment.

| Parameter of the Laser | Power(W)                       | Overlap Rate (%) | Angle (°) | Scanning Speed (mm/s) | Size of the Spot (mm) |
|------------------------|--------------------------------|------------------|-----------|-----------------------|-----------------------|
| Value                  | 600, 700, 800, 900, 1000, 1100 | 20               | 0, 10     | 15                    | 2 × 6                 |



After obtaining laser quenching samples under various operating conditions, this paper measured the hardness and thickness and analyzed the microstructure of the substrate layer, strengthening layer, and transition layer. Since the strengthening layer and transition layer were located below the surface of the sample, the quenched bearing inner ring was cut into multiple plate-like structures, and after surface grinding and polishing, the HVS-1000A microhardness tester (Wright Instruments Ltd., Beijing, China) was used for hardness testing with a test pressure of 500 gf and a holding time of 14 s. Following this, the sample underwent corrosion using a 5% nitrate alcohol solution to induce the precipitation of martensite and other microstructural constituents within the material. A detailed tissue analysis of each region of the sample was then conducted utilizing both optical microscopy (LEXT OLS5100 3D Laser Scanning Microscope, Olympus Corporation, Shanghai, China) and scanning electron microscopy techniques (SEM, JSM-IT800, JEOL Ltd., Beijing, China).

Figure 3a illustrates the overall morphology of the enhanced sample section as observed under an optical microscope, utilizing a power setting of 800 W and a laser irradiation angle of 0°. In contrast, Figure 3b presents a magnified view of the lap area captured using a 50× light lens.

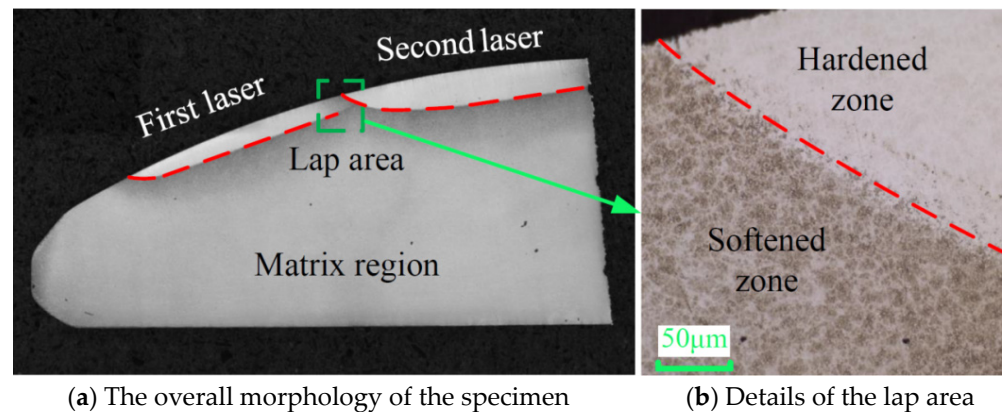


**Figure 3.** Sample under optical microscope.

In Figure 3a, a distinct stratification phenomenon is evident, characterized by the presence of a strengthening layer beneath the surface of the laser-scanned region, which exhibits an enhanced reflective effect following polishing. Beneath this intensified layer and within the overlapping regions of different laser passes lies the transition layer, which demonstrates a diminished reflective effect. The reflective properties of the underlying matrix region are marginally weaker than those of the enhanced region yet stronger than those of the transition region. In Figure 3b, the transition layer located in the lower left corner does not allow for the observation of the microscopic structure's morphology under a 50-fold magnification; however, its interface is discernible, revealing a susceptibility to erosion and a grayish-black coloration. Conversely, the reinforced layer in the upper right corner also does not permit a clear observation of the interface under 50-fold magnification, suggesting that the structural organization in this area is significantly smaller. The overall morphology of the reinforced sample after slicing under other working conditions is similar to Figure 3, except for the thickness of the reinforced transition layer.

### 2.2.2. Laser Quenching Simulation

Given that the infrared temperature camera is limited to capturing only the surface temperature of the sample during the laser hardening process, and considering that the temperature distribution within the material is critical for understanding the mechanisms

governing the hardened layer and the transition layer, the finite element simulation is used to analyze the temperature field inside the material during laser hardening. To this end, this paper uses the Workbench module of ANSYS (ANSYS 2018, ANSYS, Inc., Beijing, China) software to establish a thermodynamic coupling model of the surface laser quenching of the joint bearing, and the size of the model is shown in Figure 1. The grid is segmented using the sweeping method, resulting in an overall mesh size of 1 mm, while the local mesh size is refined to 0.1 mm, and the model has 58,000 cells after grid division. This study employs a Gaussian heat source to model the laser spot, enabling precise simulation of the energy distribution associated with the laser spot during the laser quenching process. This approach is recognized as the most prevalent method in the numerical analysis of related issues. The moving speed of the Gaussian heat source is 15 mm/s, which is consistent with the experimentation. The simulation time is 16 s, which is equivalent to two laps of laser scanning around the bearing surface, and the overlap rate is 20%. In ANSYS simulation software, the power parameter of the Gaussian heat source is energy density ( $W/mm^2$ ), so the power in Table 2 is converted by equation 1 to achieve consistency with the test light experiment.

$$\rho = \frac{P}{A} \quad (1)$$

where  $\rho$  is the energy density of the Gaussian heat source model ( $W/mm^2$ ),  $A$  is the area of the laser spot ( $mm^2$ ), and  $P$  is the power of the laser spot (W).

The thermal physical property parameters [22,23] of GCr15-bearing steel in the simulation model are set as shown in Table 3. The interpolation method is employed to analyze the physical property parameters at an unspecified temperature.

**Table 3.** GCr15 thermal property parameters of GCr15-bearing inner ring model.

| Temperature (°C)  | 20    | 200   | 400   | 600   | 800   | 1000  |
|---|-------|-------|-------|-------|-------|-------|
| Coefficient of heat conduction ( $W/m \cdot ^\circ C$ ) | 46    | 45    | 42    | 32.5  | 26    | 29    |
| Young's modulus (GPa)                                   | 201   | 179   | 163   | 103   | 87    | 67    |
| Poisson's ratio   | 0.277 | 0.269 | 0.255 | 0.342 | 0.396 | 0.490 |
| Specific heat capacity ( $J/kg \cdot ^\circ C$ )        | 560   | 650   | 780   | 880   | 860   | 780   |

When the bearing inner ring is subjected to a laser quenching test, the surface is strengthened, the two sides of the bearing are in contact with the air, and the inner surface is fixed on the live spindle. Therefore, in the numerical analysis model, the convection heat transfer between the outer surface and the two sides of the bearing inner ring and the outside air, as well as the heat transfer between the inner surface and the rotating spindle, shown in Figure 2b, are considered. The initial temperature of the sample and the environment was set at 22 °C, and the movement trajectory of the Gaussian heat source was spiral movement around the outer surface of the bearing inner ring, as shown in Figure 2b. Because the inner surface of the bearing ring is fixed in the actual laser hardening process, the outer surface is not stressed by the action of the high-energy laser beam, so the boundary condition is set to be fixed. Furthermore, the numerical model does not take into any other thermal load inputs, heat transfer conditions and constraints.

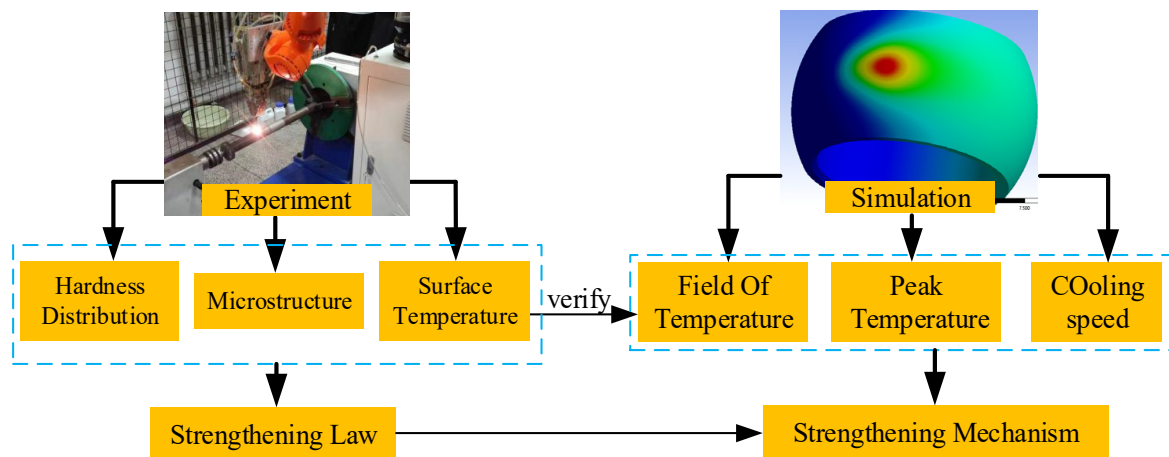
Table 4 presents a comparative analysis of the average peak temperature of the sample surface, as measured by the infrared camera during the laser quenching experiment, alongside the average peak temperature derived from simulation results at a laser irradiation angle of 0°.

**Table 4.** Peak temperature of simulation and experimental.

| Power of Laser (W)                    | 600    | 700    | 800    | 900     | 1000    | 1100    |
|---------------------------------------|--------|--------|--------|---------|---------|---------|
| Peak temperature of experimental (°C) | 840    | 927    | 948    | 974     | 1008    | 1055    |
| Peak temperature of simulation (°C)   | 821.01 | 900.36 | 930.01 | 1012.53 | 1056.14 | 1097.84 |
| Rate of deviation                     | 2.26%  | 2.87%  | 1.9%   | 3.96%   | 4.78%   | 4.06%   |

As can be seen from Table 4, the average peak temperature error between the simulation model established in this paper and the experimental results under each working condition is less than 5% (the average error was 3.305%), so it can be considered that the finite element analysis of laser quenching conducted in this paper is reliable.

The methodological framework of this study is illustrated in Figure 4. The internal hardness distribution, microstructure alterations, and surface temperature distribution of the material are obtained according to the laser quenching experiment, and these indexes are used to verify the reliability of the numerical simulation model. Then, according to the internal temperature field obtained by simulation and the experiment results, the strengthening law and mechanism of laser quenching on the outer surface of the inner ring of the GCr15 knuckle bearing were analyzed.

**Figure 4.** The methodological framework of this study. Analysis of experimental results.

### 3. Analysis of Experimental Results

#### 3.1. Hardness

The most apparent enhancement in the material's properties resulting from laser quenching is the increase in hardness. In this paper, the hardness of the sample was tested along the depth direction and the arc edge direction. The arc edge measurement starting point was about 1 mm away from the laser scanning area, and the depth direction measurement starting point was about 0.05 mm away from the sample surface, as shown in Figure 5.

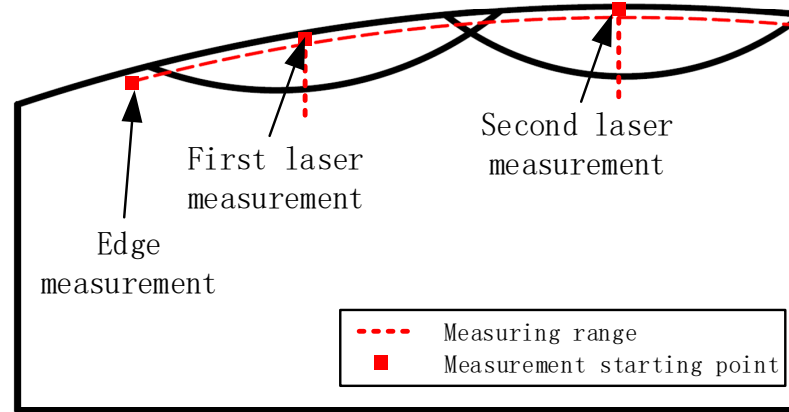


**Figure 5.** Measurement method of the sample's hardness.

Since the fluctuation of hardness distribution in the hardening zone of the sample, the single measurement result cannot reflect the real hardening degree of the sample. For the sample obtained under each working condition, the hardness of the hardening zone was tested 10 times in this paper. The hardness and value of each sample's hardening zone produced by the first and second lasers are shown in Figure 6a. Figure 6b shows the thickness of the strengthened zone after the first and second laser scanning in each working condition.

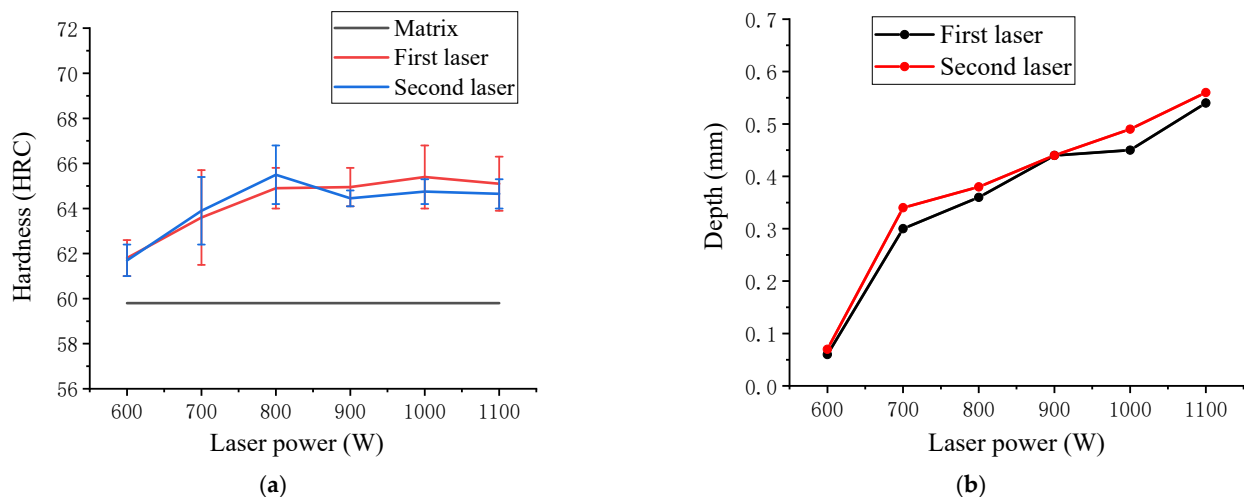


**Figure 6.** Variation of sample hardness with laser power. (a) Relationship between hardness and laser power. (b) Relationship between hardening layer's depth and laser power.

As illustrated in Figure 6a, the hardening effect induced by low-power (600 W) laser scanning on bearing samples is minimal, resulting in a hardness value that is approximately 2 HRC higher than that of the base material; meanwhile, the thickness of the hardened layer is less than 0.1 mm.

The enhancement of laser power leads to a marked improvement in the hardening effect of the sample, resulting in a hardness increase of 5–8 HRC compared to the matrix. Additionally, the thickness of the hardened layer expands to a range of 0.3–0.6 mm. This is due to the low energy density resulting from the lower laser power output, which can only create a small high-temperature area on the surface of the sample. As a result, the sample only reaches above Ac1 (Phase Transformation Temperature 1) for GCr15 material at a depth of within 0.1 mm, leading to a thinner hardened layer. The hardness value and thickness of the hardened layer produced by the first and second laser scanning are relatively close, which indicates that the cumulative effect of heat in the laser scanning



process has less impact on the strengthening effect, which is an obvious characterization of the acute cooling and heating effect of laser energy on the surface of the material.

It can be seen from Table 4 that the peak temperature of the hardened sample increases with the increase of laser power. At 900 W, the peak temperature of the sample after laser quenching can reach 974 °C, and at 1000 W, this data surpasses 1000 °C. GCr15-bearing steel would have a serious decarbonization phenomenon when the surface temperature is higher than 1000 °C, which makes its surface performance decline [24]. The weaker antioxidant capacity is one of the characteristics of the decarbonization of materials. In this study, it has been observed that with the increase of laser power, the degree of oxidation on the surface of the material increases. Simultaneously, at low power, as shown in Figure 6, the increase in hardness of the strengthened layer is minimal, and the thickness of the strengthened layer is also limited. In conclusion, to adequately consider the surface quality and the strengthening effects of the material, it is essential to regulate the laser power within the range of 800 W to 900 W for the subject of this study.

Figures 6b and 7a are the hardness test results along the depth direction and the edge direction when the laser power is 900 W and the laser irradiation angle is 0°, respectively; Figures 6d and 7c are the hardness test results along the depth direction and the edge direction when the laser power is 900 W and the laser irradiation angle is 10°, respectively.

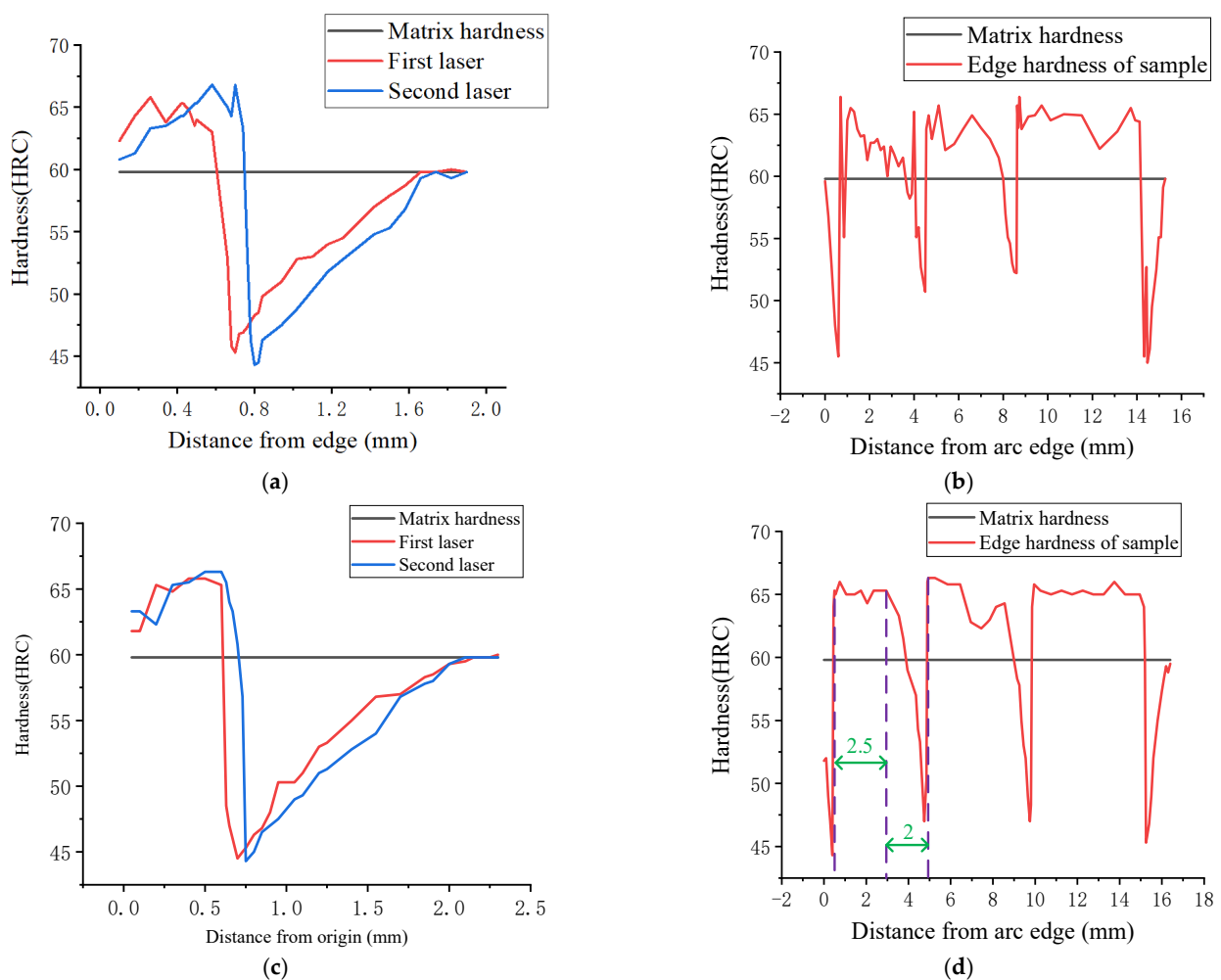


**Figure 7.** Hardness distribution inside the sample. (a) The hardness test results along the depth direction (900 w, 0°). (b) The hardness test results along the edge direction (900 w, 0°). (c) The hardness test results along the depth direction (900 w, 10°). (d) The hardness test results along the edge direction (900 w, 10°).

The hardness distribution trend of the samples under other working conditions is similar to the results shown in Figure 7: in the depth direction, the hardening layer begins to occur about 0.05 mm below the surface, and the change of hardness peak is shown in Figure 5. As shown in Figure 7, the hardness values of the hardened layer exhibit certain fluctuations. This is due to the fact that the metal microstructure prior to hardening has certain differences in different microscopic areas, such as the degree of retained austenite and the carbon content. These factors can all affect the hardening effect of laser quenching. Below the hardened layer is a transition zone, where the hardness value is reduced and the thickness is about 1–1.5 mm. Below the transition zone is the matrix zone, and the hardness value has no obvious change compared with that before strengthening. The hardness measurement results along the arc edge show that the hardness of the strengthened zone can reach 62.5–66 HRC. Similar to the measurement results along the depth direction, the hardness of the strengthened zone also has a certain degree of fluctuation along the arc edge.

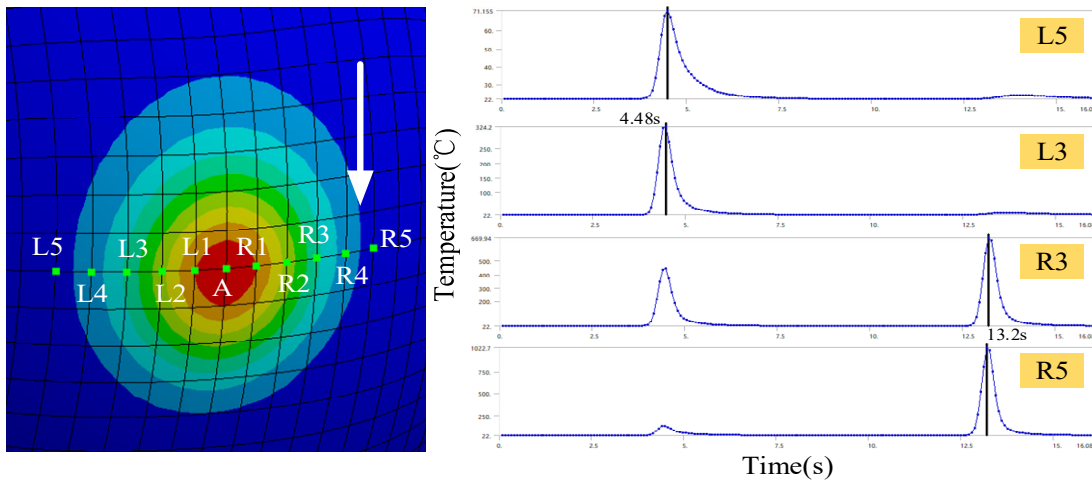
By comparing Figure 7a,c, it can be found that the hardness value in the depth direction of the sample's strengthened region is maintained at a higher level to a greater extent after the use of an inclined laser. Similarly, it can be seen from Figure 7b,d that the inclined laser angle also makes the hardening zone of the material maintain a higher level along the arc edge to a greater extent. However, the inclined laser does not make the hardness peak in the hardening zone, and the hardness valley in the transition zone has significant changes. Meanwhile, the thickness and width of the hardening layer are not significantly different from that of the direct laser. This phenomenon may be attributed to the inclination of the laser, which results in a wider projection of the laser beam on the material's surface. Thus, the laser quenching time and the energy density obtained in the unit area of the material are slightly affected. As a result, the absorption rate of the laser energy by the material is altered. However, based on the aforementioned findings, this alteration appears to enhance the effectiveness of the laser quenching process.

### 3.2. Strengthening Mechanism of Sample

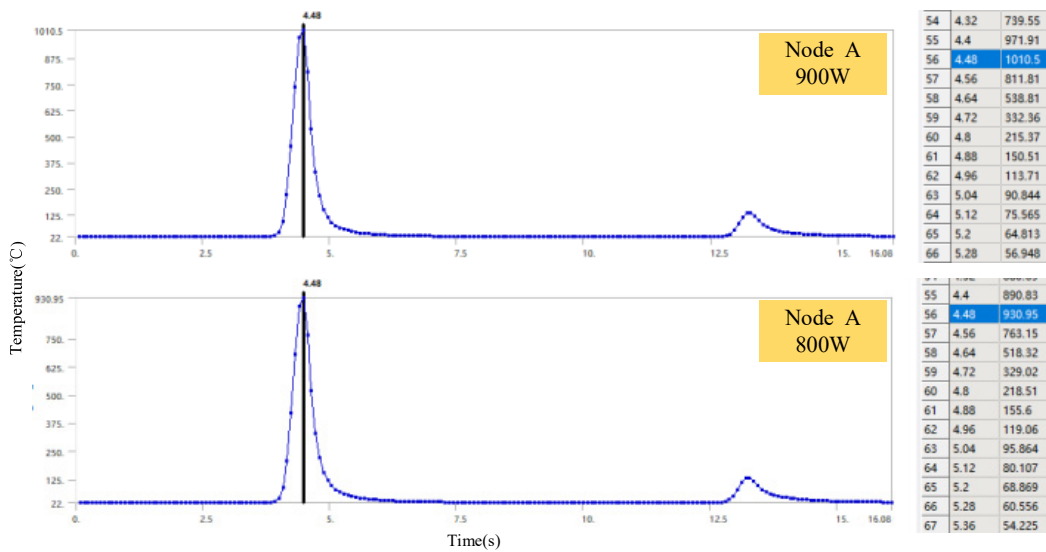
The enhanced region in Figure 3a shows a fusiform with two ends narrower than the middle. This is because the laser spot is subject to Gaussian distribution to a certain extent. That is, the energy density generated by the laser in the central region is greater than that in the edge region. The heat in the edge region scanned by the laser diffuses to the matrix and the center at the same time, making the energy loss rate in the central region lower than that in the edge region. This creates a thicker layer of heat zone.

#### 3.2.1. Strengthening Mechanism in Edge Direction

Figure 8a shows the laser spot of 900 W scanning on the bearing's surface. During the scanning process, the laser spot was comet-like, the time of intercept was 4.48 s, and the central temperature of the laser spot was 1010.5 °C, which was much higher than the Ac1 temperature of GCr15 material (around 730 °C). In order to obtain the temperature distribution law on the material's surface during laser quenching, this paper processed the simulation results and extracted 11 nodes, as shown in Figure 8a, from the material's surface. The distance of nodes on the left side of node A is 1.2 mm, and the distance of nodes on the right side is 1 mm. Figure 8b illustrates the temporal variation in instantaneous temperature for nodes L5, L3, R3, and R5 when subjected to a power input of 900 W. Figure 8c depicts the temporal variation in instantaneous temperature at node A under power inputs of 900 W and 800 W. At 4.48 s, the center of the laser spot is positioned at node A. At 13.2 s, the center of the laser spot moves to node R5.



(a) The Selection method of nodes L5~R5 (b) The change of instantaneous temperature of nodes L5, L3, R3, and R5



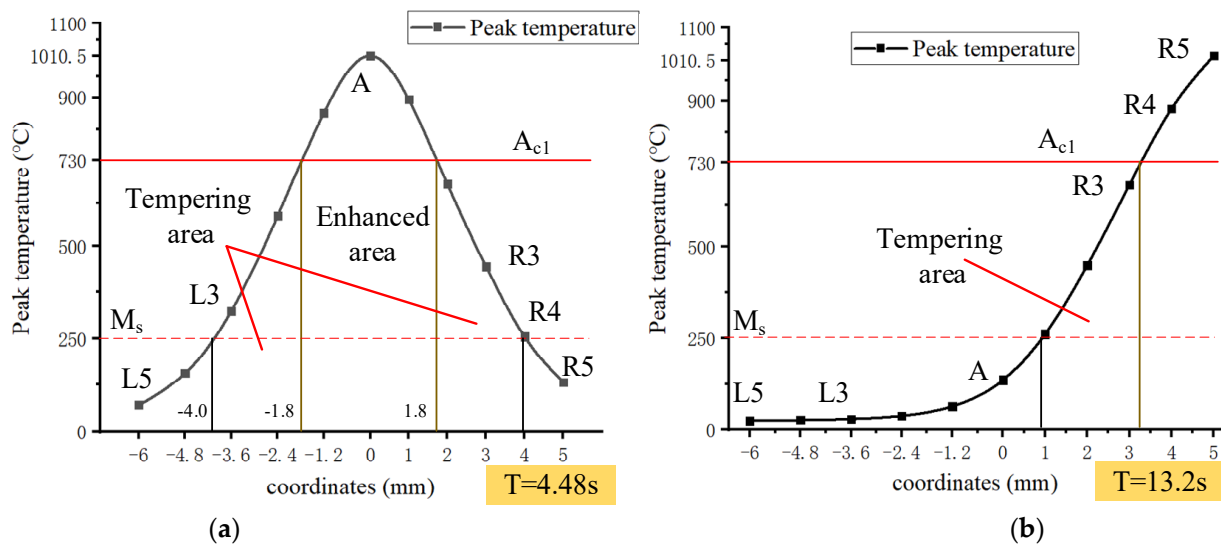
(c) The change of node A's instantaneous temperature with time (800 W and 900 W)

Figure 8. Results of the laser quenching simulation.

According to the simulation results, all nodes in Figure 8a have relatively drastic temperature fluctuations near 4.48 s and 13.2 s, in which the peak temperature of nodes L5~R2 is near 4.48 s, and that of nodes R3~R5 is near 13.2 s, and the temperature of these nodes is basically stable below 40 °C in the rest time. The second peak temperature fluctuation of node A at 12.9~13.8 s is 127 °C, which is the temperature increase caused by the second laser scan to the similar position of the model surface, but this temperature is no longer enough to affect the material's properties. Other nodes also have similar situations, but the temperature fluctuation is smaller. The temperature change trend at node R5 shows a peak temperature fluctuation of 141 °C around 4.48 s, which is the heat generated when the laser spot moves to the vicinity of node A. In the vicinity of 13.2 s, it produced a second temperature fluctuation, and the peak temperature reached 1010.5 °C. The above phenomenon shows that in the laser quenching process using the overlap process, the hot zone generated by different passes of the laser will have a certain mutual influence.

The Ms (Martensite Start temperature) of GCr15 material is generally between 200 and 300 °C, with 250 °C specified in this paper. The Ac1 temperature in this paper is 730 °C, so it can be considered that the bearing inner ring used in this paper will experience varying degrees of tempering within the range of 250 to 730 °C. Combined with these characteristic temperatures and node temperature data in Figure 8, the temperature distribution curves

of the sample's surface at 4.48 s and 13.2 s under 900 W power are shown in Figures 8b and 9a. The horizontal coordinate in Figure 9 is the position of nodes L5~R5 in Figure 8a, node A is the coordinate point 0, and the node of L5 to R1 is negative. The nodes of R1 to R5 are positive.



**Figure 9.** Hardness distribution on the surface of the sample. (a) The temperature distribution curves of the sample's surface at 4.48 s. (b) The temperature distribution curves of the sample's surface at 13.2 s.

As can be seen from Figure 9a, when the laser spot is scanned to node A, the temperature decreases on both sides of it, and the temperature reaches  $A_{c1}$  at a distance of 1.8 mm from the center of the heat source under the power of 900 W. The hot zone generated by the laser spot is approximately symmetrically distributed; therefore, the width of the strengthened zone generated on the material surface is about 3.6 mm. In Figure 9a, the peak temperature of the material in the region of about 1.8~4 mm from the center of the laser spot is 250~730 °C, which is in the high-temperature tempering and medium-temperature tempering interval of the GCr15 material, and the material would undergo a certain degree of tempering phenomenon leading to a decrease in hardness and strength. As can be seen from Figure 9b, at the moment of 13.2 s, the width of the intensified zone produced by the laser spot on the left side of node R5 is about 1.8 mm, so the width of the intensified zone on both sides of the node should be about 3.6 mm. The tempering zone on the left side of node R5 is at a distance of about 1~3.2 mm from node A, which suggests that the second laser will cause the intensified zone created by the first laser to undergo tempering, and the width of the intensified zone produced by the first laser will be narrower than the 3.6 mm shown in Figure 9a. In order to verify this inference, the material's surface temperature distribution curves at 4.48 s and 13.2 s were superimposed, and the actual distribution of the tempering zone and strengthening zone near the first laser under 900 W power was finally obtained, as shown in Figure 10a. Figure 10b shows the comparison between the actual and predicted results of the width of the strengthening zone and tempering zone generated by the first laser at 900 W, where the actual width is based on the hardness change. As shown in Figure 7d, the stable hardness enhancement area produced by the first laser at 900 W is the hardened zone, with a width of 2.4 mm; the interval where the hardness starts to decrease until the beginning of the next hardness peak is the tempered zone, with a width of 2 mm.

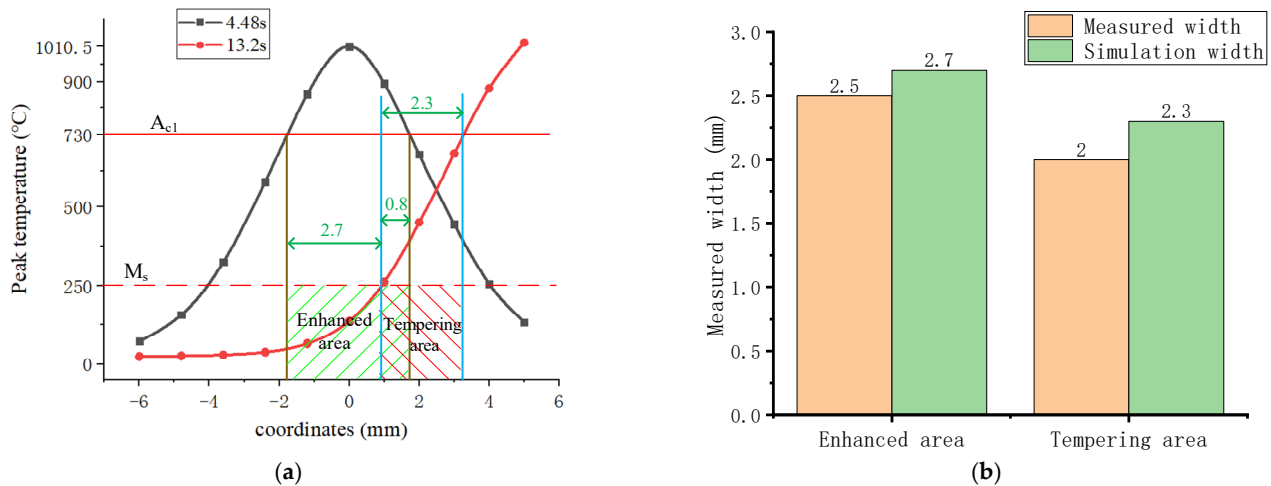


**Figure 10.** Prediction of the width of the strengthening and tempering area. (a) Prediction of the distribution of enhanced area and tempering area on the sample's surface. (b) The width of the enhanced area and tempering area in actual and predicted results.

As can be seen from Figure 10, the simulation results for the width of the reinforcement layer and the tempering layer are relatively reliable, with an error rate of 8% and 15%, respectively, which indicates that the presumption that the GCr15 material is strengthened above the temperature of  $A_{c1}$  is correct, and it also proves that if the tempering zone generated by the subsequent laser is located in the strengthened zone of the previous laser, it will lead to the tempering phenomenon of the strengthened zone, which is harmful to the strengthening effect of laser quenching. Furthermore, owing to the energy properties of the laser, the temperature on its two sides will invariably be lower than that of the central region. When this temperature falls below the  $A_{c1}$  temperature of the material, it induces a tempering effect in those areas. Consequently, when employing laser quenching technology to enhance material properties, it is advisable to utilize a laser spot that is as large as feasible to ensure the temperature in the heated zone on the material's surface attains or exceeds its  $A_{c1}$  temperature.

### 3.2.2. Strengthening Mechanism in Depth Direction

Figure 11a shows the model cross section when the laser spot is located at node A in Figure 8 and selects nodes from node A into the material and extracts the temperature at each node, with each node spaced 0.1 mm apart. The obtained node temperature profile trends are all consistent with that of node A in Figure 8c. The peak temperature distribution curve in the material's strengthening zone along the depth direction, based on the peak temperature of nodes from nodes A~A0.7 (which appeared at 4.48 s), is shown in Figure 11b. In Figure 11b, the horizontal axis represents the depth with node A as the reference point (0 position) and extends towards node A0.7.

As illustrated in Figure 11b, the intersection points of the  $A_{c1}$  temperature of the GCr15 material and the two peak temperature curves are located at 0.325 mm and 0.422 mm, respectively. Based on the analysis above, this depth should correspond to the peak depth of the enhanced zone produced by the first laser shown in Figure 3a. The measured data, as shown in Figure 6b, are 0.36 mm and 0.44 mm, respectively. This indicates that the simulation results have an error within 10%, thus confirming that this inference is correct.



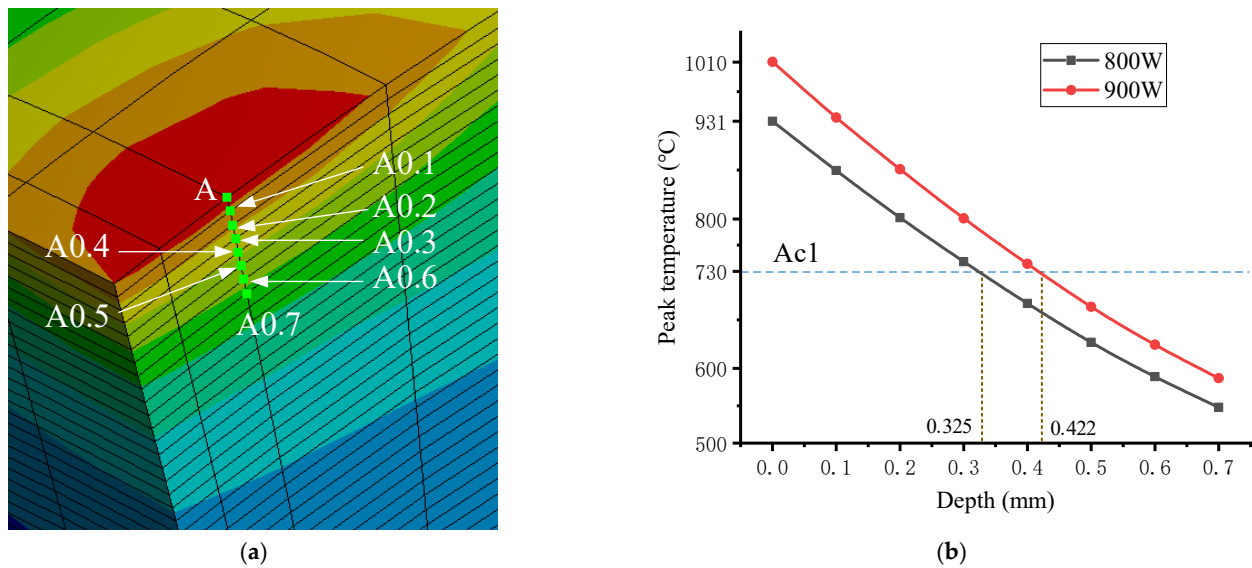


**Figure 11.** The temperature distribution in the strengthening zone along the depth direction. (a) The Selection method of nodes A~A0.7. (b) The peak temperature distribution curve in the material’s strengthening zone along the depth direction.

### 3.2.3. Cooling Process of Laser Quenching

As demonstrated in Figure 8c, at a power of 900 W, node A attains its maximum temperature of 4.48 s. At 4.8 s, its temperature drops below the Ms point, reaching 215.37 °C within a duration of 0.32 s. Thereafter, a decline to 39.866 °C is observed at 5.6 s, denoting that the cooling process is basically complete. The cooling process at 800 W laser power is similar, with only a slight reduction in peak temperature. During the quenching process of steel, a faster cooling rate can result in finer martensite particles, effectively hindering the movement of dislocations, thereby improving the mechanical properties of the material and increasing its strength and hardness. Regarding carbides: at high temperatures, carbides in steel would dissolve in austenite. During the cooling process, a faster cooling rate can suppress the diffusion and rearrangement of carbon atoms in the steel, thereby reducing the precipitation of carbides and resulting in smaller carbide particle sizes, which, in turn, enhances the hardness and strength of the material.

The speed of cooling of the material during a continuous change is calculated in the manner of Equation (2):

$$v(t) = \frac{dT}{dt} \tag{2}$$

where  $v$  is the material cooling speed (°C/s),  $T$  is the temperature (°C),  $t$  is the time (s).

While the laser quenching simulation data obtained in this paper are discrete, the material cooling speed at time  $i$  is calculated in the manner of Equation (3):

$$v_i = \frac{T_i - T_{i-1}}{t_i - t_{i-1}} \tag{3}$$

Figure 12a shows the temperature changes at node A from 3.92 to 5.6 s under 800 W and 900 W conditions; Figure 12b shows the cooling speed changes during this period, which is obtained from Equation (3). In Figure 12b, a positive cooling speed indicates that the material is in a heating process, while a negative cooling speed indicates that the material is in a cooling process.

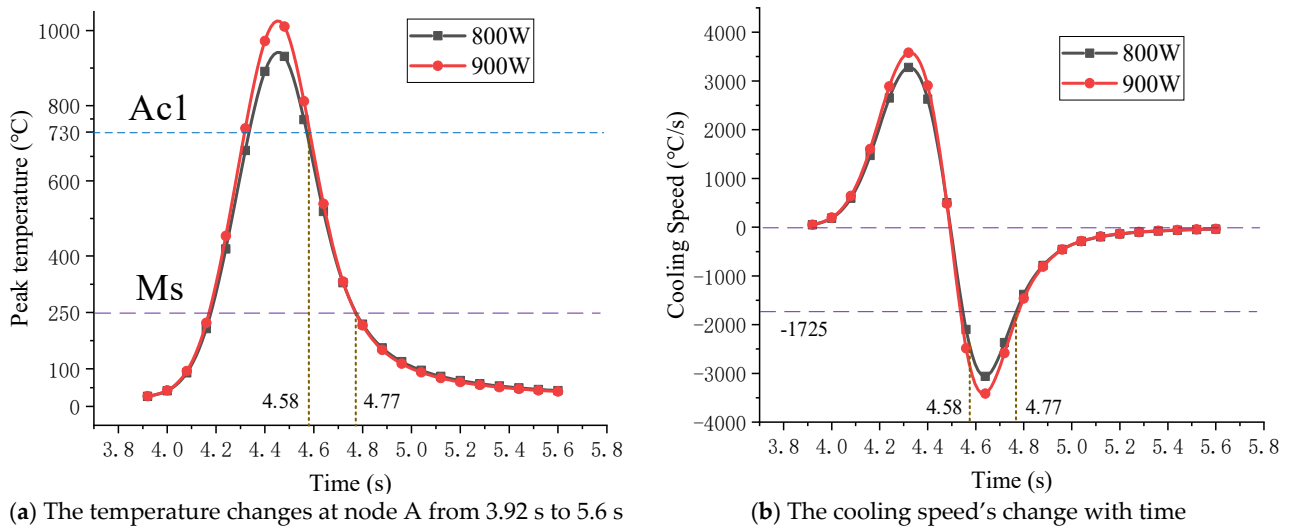


**Figure 12.** The material's surface temperature and the cooling speed.

Analysis of Figure 12b reveals that the cooling speed trends under laser conditions of 900 W and 800 W exhibit similarities, with peak occurrences aligned temporally. Notably, the peak cooling speed at 900 W is marginally faster compared to that at 800 W. This phenomenon can be attributed to the positive correlation between the coefficients of the three modes of heat transfer (convection, conduction, and radiation) and the temperature differential. Since the peak surface temperature of the material at 900 W surpasses that at 800 W, the temperature difference between the surface and the surrounding environment is greater at approximately 4.48 s, thereby facilitating a more rapid cooling speed. Furthermore, as illustrated in Figure 12a, the time for the material to attain Ac1 and Ms temperatures are approximately 4.58 s and 4.77 s, respectively. During the interval from 4.58 to 4.77 s, as depicted in Figure 12b, the cooling speed of the material consistently exceeded 1700 °C/s, with the peak cooling speed surpassing 3000 °C/s, which is considerably higher than that achieved through conventional quenching methods.

#### 3.2.4. The Sample's Microstructure

Figure 13a–c show the SEM scanning images of the hardened zone, tempering zone, and matrix zone of the GCr15 bearing inner ring obtained at a power of 900 W. The areas marked with green frames indicate martensite, while those marked with red frames indicate carbides.

From Figure 13, it can be seen that the main microstructural components of the GCr15 bearing inner ring before strengthening (Figure 13c) are martensite and oval-shaped carbides. The martensite structure is irregular, primarily consisting of lath and coarse needle shapes, with a size of approximately  $0.6 \pm 0.2 \mu\text{m}$ . There are a considerable number of carbides, with a size of about  $0.75 \pm 0.2 \mu\text{m}$ .

The hardened zone produced by laser quenching (Figure 13a) contains a mere few carbides. The size of the martensite structure in the hardened zone is slightly smaller than that in the matrix zone, with the structure primarily being lath-shaped. The mechanism behind this is that after the material reaches its Ac1 temperature, the carbides in the structure begin to dissolve. However, since this process is relatively short, lasting only about 0.3 s, there are still some carbides that remain undissolved. Subsequently, the cooling speed exceeding 1700 °C/s effectively suppresses the growth of carbides while also making the resulting martensite structure denser, thus creating a hardened zone with higher hardness and strength than the matrix.

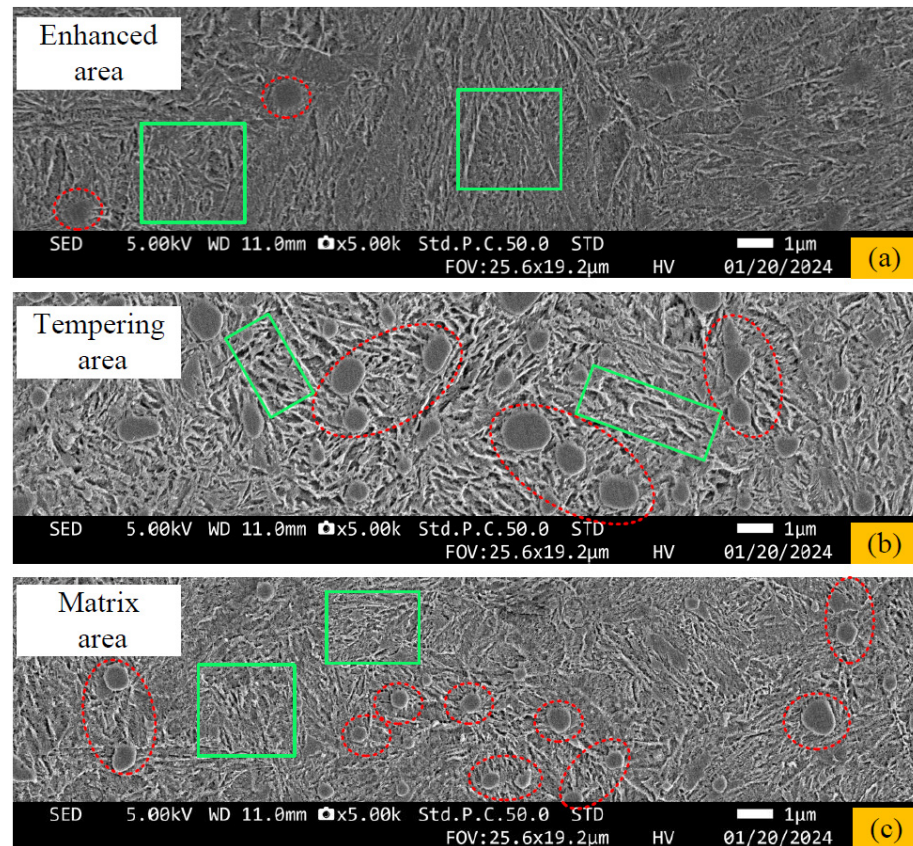


**Figure 13.** Microstructure of each region of the sample. (a) The SEM scanning images of the hardened zone. (b) The SEM scanning images of the tempering zone. (c) The SEM scanning images of the matrix zone. (The areas marked with green frames indicate martensite, while those marked with red frames indicate carbides).

In the tempered zone (Figure 13b), the martensite structure appears coarser, with a size of approximately  $0.8 \pm 0.2 \mu\text{m}$ , primarily exhibiting a coarse needle appearance. The number of carbides is similar to that in the matrix zone, but their size is larger, about  $1 \pm 0.3 \mu\text{m}$ . This microstructure is caused by laser quenching which makes the temperature of these regions within the tempering temperature range of the GCr material.

The presence of smaller carbide dimensions and a finer martensitic microstructure within the strengthened region serves to impede dislocation motion, consequently enhancing the material's resistance to deformation, as well as its hardness and wear resistance. Conversely, the occurrence of larger carbide sizes and a coarser martensitic structure in the tempering region leads to a degradation of the mechanical properties and a reduction in hardness.

#### 4. Conclusions

This study focuses on the laser quenching treatment of the inner ring of GCr15 knuckle bearings, accompanied by the development of a numerical simulation model to simulate this process. Through the analysis of the experimental results and numerical model, the following main research results are obtained:

- (1) After laser quenching, the GCr15 bearing material exhibits a strengthened zone and a tempered zone in the depth and arc edge directions. The strengthened zone demonstrates a higher hardness, smaller martensite size, and a lower concentration of carbides relative to the matrix. In contrast, the tempered zone exhibits a lower hardness and a larger size of martensite and carbides compared to the matrix.

- (2) The numerical simulation model of the laser quenching process established in this paper is highly reliable. Through an analysis of the model in comparison with experimental data, it has been demonstrated that the region of the material's surface above the Ac1 temperature experiences a strengthening effect, whereas the region between the Ac1 and Ms temperatures undergoes a certain degree of tempering.
- (3) For the subject of this study, an appropriate angle of inclination can enhance the stability of the hardening effect in the hardened zone of the material; laser quenching at power levels between 800 W and 900 W exhibits favorable results, where the cooling speed of the material exceeds 1700 °C/s prior to reaching the Ms temperature.
- (4) In the laser quenching process employing the overlap method, the hot zones generated by different laser passes will have a certain degree of interaction, which may cause the hardened zone produced by the previous laser to temper again.

In conclusion, laser quenching is capable of generating a hardened surface layer characterized by increased hardness and a finer microstructure. However, it is important to acknowledge that the mechanical properties of the tempering zone created by laser quenching are inferior to those of the base material. When employing laser lap techniques, particular attention should be given to the tempering effects observed in the lap region. Furthermore, it is advisable to utilize a tilted laser at a small angle during production, as this approach may enhance the stability of the strengthening effect.

**Author Contributions:** Conceptualization, X.Y. and H.Z.; methodology, H.Z. and X.M.; software, D.J. and M.C.; validation, M.C. and X.M.; investigation, X.Y.; resources, X.Y.; data curation, H.Z.; writing—original draft preparation, M.C.; writing—review and editing, H.Z.; supervision, D.J.; project administration, D.J.; funding acquisition, H.Z. All authors have read and agreed to the published version of the manuscript.

**Funding:** This research was funded by the National Key Research and Development Plan (Grant No. 2021YFB2011000); the Longmen Laboratory tuyere industry project (Grant No. LMFKCY2023001); the Frontier Exploration Project of Longmen Laboratory (Grant No. LMQYTSKT037); and the Key Scientific and Technological Project of Henan Province (Grant No. 242102220081).

**Institutional Review Board Statement:** Not applicable.

**Informed Consent Statement:** Not applicable.

**Data Availability Statement:** The research data are all included in the article.

**Conflicts of Interest:** Author Xiuli Yang and Maolin Cheng were employed by the company CCCC Second Harbor Engineering Co., Ltd. The remaining authors declare that the research was conducted in the absence of any commercial or financial relationships that could be construed as a potential conflict of interest.

## References

1. Rodiouchkina, M.; Lind, J.; Pelcastre, L.; Berglund, K.; Rudolphi, Å.K.; Hardell, J. Tribological behaviour and transfer layer development of self-lubricating polymer composite bearing materials under long duration dry sliding against stainless steel. *Wear* **2021**, *484*, 204027. [[CrossRef](#)]
2. Rodiouchkina, M.; Lindsjö, H.; Berglund, K.; Hardell, J. Effect of stroke length on friction and wear of self-lubricating polymer composites during dry sliding against stainless steel at high contact pressures. *Wear* **2022**, *502*, 204393. [[CrossRef](#)]
3. Hua, J.; Liu, J.; Liu, P.; Zhao, X.; Chen, C.; Ren, R. Investigation on WEA fatigue spalling of U71MnG rail material subject to laser quenching surface treatment. *Wear* **2023**, *512–513*, 204560. [[CrossRef](#)]
4. Hua, J.; Liu, J.; Liu, F.; Liu, P.; Zhao, X.; Ren, R. Study on strip WEA wear damage and fatigue spalling of U71MnG rail material by laser quenching treatment. *Tribol. Int.* **2022**, *175*, 107811. [[CrossRef](#)]
5. Li, Z.X.; Tong, B.Q.; Zhang, Q.L.; Yao, J.H.; Kovalenko, V.; Li, Z.G. Influence of initial micro-structure on the microstructure evolution and mechanical properties of 1.0 C-1.5 Cr steel in the laser surface quenching. *Mater. Sci. Eng. A* **2020**, *788*, 139490. [[CrossRef](#)]



6. Li, Z.-X.; Tong, B.-Q.; Zhang, Q.-L.; Yao, J.-H.; Kovalenko, V. Microstructure refinement and properties of 1.0C-1.5Cr steel in a duplex treatment combining double quenching and laser surface quenching. *Mater. Sci. Eng. A* **2020**, *776*, 138994. [[CrossRef](#)]
7. Cao, X.; Shi, L.; Cai, Z.; Liu, Q.; Zhou, Z.; Wang, W. Investigation on the microstructure and damage characteristics of wheel and rail materials subject to laser dispersed quenching. *Appl. Surf. Sci.* **2018**, *450*, 468–483. [[CrossRef](#)]
8. Zong, X.; Li, Z.; Li, J.; Cheng, X.; Tang, H.; Wang, H. Non-isothermal  $\beta$  grain growth behaviour of pure titanium under laser quenching. *Mater. Sci. Technol.* **2020**, *36*, 668–673. [[CrossRef](#)]
9. Yasuda, T.; Kaisho, M.; Nishimoto, K.; Okumoto, Y. Monitoring of Laser Quenching of the Carbon Steel by Acoustic Emission. *Mater. Transact.* **2023**, *64*, 604–612. [[CrossRef](#)]
10. Chen, S.Y.; Chen, Y.X.; Jiao, S.F.; Zhong, L.; Gao, L.; Miao, L. Study on laser surface quenching structure and hardness of C45 steel. *Metalurgija* **2021**, *60*, 253–256.
11. Zhang, Y.Y.; Chen, Y.X. Rapid optimization of laser quenching process based on bp neural network. *Metalurgija* **2023**, *62*, 68–70.
12. Han, X.; Li, C.; Zhang, D.; Li, Y.; Gao, X. Numerical simulation and experiment of quenching process of 35CrMnSi by disk laser. *J. Laser Appl.* **2021**, *33*, 022004. [[CrossRef](#)]
13. Yu, Z.; Li, C.; Chen, Z.; Li, Y.; Han, X. Sensitivity Analysis of Laser Quenching Parameters of ASTM 1045 of Disk Laser Based on Response Surface Method. *Met. Mater. Int.* **2021**, *27*, 1236–1251. [[CrossRef](#)]
14. Chen, Z.; Zhu, Q.; Wang, J.; Yun, X.; He, B.; Luo, J. Behaviors of 40Cr steel treated by laser quenching on impact abrasive wear. *Opt. Laser Technol.* **2018**, *103*, 118–125. [[CrossRef](#)]
15. Ping, X.L.; Fu, H.G.; Wang, K.M.; Sun, S.T.; Ju, J.; Lin, J.; Yu, D.; Xing, Z.; Lei, Y.P. Effect of laser quenching on microstructure and properties of the surface of track materials. *Surf. Rev. Lett.* **2018**, *25*, 1950030. [[CrossRef](#)]
16. Li, C.; Gao, H.; Chen, X.; Liu, Z.; Han, X. Study on Multi-Field Coupled Evolution Mechanism of Laser Irradiated 40Cr Steel Quenching Process Based on Phase Change Induced Plasticity. *Met. Mater. Int.* **2021**, *28*, 1919–1937. [[CrossRef](#)]
17. Chen, Y.; Zhao, X.; Liu, P.; Pan, R.; Ren, R. Influences of local laser quenching on wear performance of D1 wheel steel. *Wear* **2018**, *414–415*, 243–250. [[CrossRef](#)]
18. Yao, Q.; Tian, C.; Sun, J.; Zuo, L.; Tong, W. Microstructure and properties of nitrided layer of titanium plate, produced by simultaneous laser quenching and liquid-nitrogen cryogenics. *Sci. China Technol. Sci.* **2018**, *61*, 1901–1906. [[CrossRef](#)]
19. Zhan, K.; Zhang, Y.; Bao, L.; Yang, Z.; Zhao, B.; Ji, V. Surface characteristic and wear resistance of QT-700-2 nodular cast iron after laser quenching combing with shot peening treatment. *Surf. Coat. Technol.* **2021**, *423*, 127589. [[CrossRef](#)]
20. Sundqvist, J.; Manninen, T.; Heikkinen, H.-P.; Anttila, S.; Kaplan, A. Laser surface hardening of 11% Cr ferritic stainless steel and its sensitisation behaviour. *Surf. Coat. Technol.* **2018**, *344*, 673–679. [[CrossRef](#)]
21. Šebek, M.; Falat, L.; Kováč, F.; Petryshynets, I.; Horňák, P.; Girman, V. The Effects of Laser Surface Hardening on Microstructural Characteristics and Wear Resistance of AISI H11 Hot Work Tool Steel. *Arch. Met. Mater.* **2017**, *62*, 1721–1726. [[CrossRef](#)]
22. Hu, L.; Li, B.; Pueh, L.H.; Wang, Z.; Wang, Y. Effect of single/multi-particle grinding parameters on surface properties of bearing steel GCr15. *Eng. Sci. Technol. Int. J.* **2024**, *58*, 101851. [[CrossRef](#)]
23. Li, Z.; Wen, Z.; Su, F. Modeling research on laser quenching process of GCr15 bearing steel basing on material properties obtained with experimental methods. *Mater. Res. Express* **2021**, *8*, 096516. [[CrossRef](#)]
24. Wang, H.; Su, F.; Wen, Z. Study on decarburization mechanism and law of GCr15 bearing steel during heat treatment. *Adv. Mater. Sci. Eng.* **2022**, *2022*, 3723680.

**Disclaimer/Publisher’s Note:** The statements, opinions and data contained in all publications are solely those of the individual author(s) and contributor(s) and not of MDPI and/or the editor(s). MDPI and/or the editor(s) disclaim responsibility for any injury to people or property resulting from any ideas, methods, instructions or products referred to in the content.